From: Mark Kirk / LCS
To: Steven Long
Date: 7/3/02 4:13PM
Subject: Fwd: Failure Model for DB

Steve -

Attached please find a report from ORNL regarding the state of their model of DB in the "as found" condition. Paul is currently putting the finishing touches on this report (please consider the attached only a draft).

The short summary of this report is as follows:

1. If we use a Weibull cumulative probability function to represent the uncertainty associated with the failure criteria we arrive at a predicted lower bound burst pressure of 6.65 ksi. Because the 3 parameter Weibull function has a finite lower bound value there is - according to this model - zero probability of failure at pressures below 6.65 ksi

2. If instead we adopt a Normal cumulative probability function to represent the uncertainty associated with the failure criteria we arrive at a cumulative probability of failure of 8.4E-10 at the operating pressure of 2.165 ksi. At a slight overpressure (2.5 ksi) the probability of failure goes up by about an order of magnitude to 8.9E-9. In either event, these are very small numbers.

Next week we will begin calculations on larger footprints for the wastage area

Mark

CC: Bass, Richard - ORNL; Edwin Hackett; Nilesh Chokshi; Wallace Norris; Williams, Paul - ORNL

ORNL/NRC/LTR-

Contract Program or Project Title:	Heavy-Section Steel Technology (HSST) Program
Subject of this Document:	Analysis of the Davis-Besse RPV Head Wastage Area and Cavity
Type of Document:	Letter Report
Authors:	P. T. Williams B. R. Bass
Date of Document:	September 2002
Responsible NRC Individual and NRC Office or Division	M. T. Kirk Division of Engineering Technology Office of Nuclear Regulatory Research

Prepared for the
U. S. Nuclear Regulatory Commission
Washington, D.C. 20555-0001
Under Interagency Agreement DOE 1886-N653-3Y
NRC JCN NoY6533

OAK RIDGE NATIONAL LABORATORY
Oak Ridge, Tennessee 37831-8056
managed and operated by
UT-Battelle, LLC for the
U. S. DEPARTMENT OF ENERGY
under Contract No. DE-AC05-00OR22725

ORNL/NRC/LTR-

Analysis of the Davis-Besse RPV Head Wastage Area and Cavity

P. T. Williams
B. R. Bass

Oak Ridge National Laboratory
Oak Ridge, Tennessee

Manuscript Completed – September 2002
Date Published –

Prepared for the
U.S. Nuclear Regulatory Commission
Office of Nuclear Regulatory Research
Under Interagency Agreement DOE 1886-N653-3Y

NRC JCN No. Y6533

OAK RIDGE NATIONAL LABORATORY
Oak Ridge, Tennessee 37831-8063
managed and operated by
UT-Battelle, LLC for the
U. S. DEPARTMENT OF ENERGY
under Contract No. DE-AC05-00OR22725

CAUTION

This document has not been given final patent clearance and is for internal use only. If this document is to be given public release, it must be cleared through the site Technical Information Office, which will see that the proper patent and technical information reviews are completed in accordance with the policies of Oak Ridge National Laboratory and UT-Battelle, LLC.

Analysis of the Davis-Besse RPV Head Wastage Area and Cavity

P. T. Williams and B. R. Bass
Oak Ridge National Laboratory
P. O. Box 2009
Oak Ridge, TN, 37831-8056

Abstract

In support of ongoing investigations by the United States Nuclear Regulatory Commission's (NRC) Office of Nuclear Regulatory Research, the Heavy-Section Steel Technology Program at Oak Ridge National Laboratory has carried out structural analyses of the damaged reactor pressure vessel (RPV) head located at the Davis-Besse Nuclear Power Station. This report presents the results of a finite-element analysis of the wastage area using submodeling techniques. A bounding case for the "as-found" condition of the cavity is developed and analyzed under static pressure loading conditions up to the point of failure. The specific failure mode addressed by this analysis is *incipient tensile plastic instability* (i.e., plastic collapse) of the cladding. Wastage-area growth scenarios are also postulated based on assumed *self-similar* and *ellipsoidal* growth patterns, and the amount of exposed cladding surface area required to produce failure down to the nominal reactor coolant system (RCS) operating pressure is estimated for each growth pattern. Comparisons are made between the finite-element computational results and the burst pressure predictions from a theoretical model (*center-membrane theory* of Chakrabarty and Alexander (1970)) of failure in circular diaphragms under lateral pressure loading. A stochastic model, presented in an earlier report [1], is also applied to provide probabilistic estimates of the predictive uncertainty of the computational results.

For the bounded "as-found" case, the median predicted burst pressure, $BP_{0.5}$, is 7.36 ksi for a cladding thickness of 0.24 in. and 5.73 ksi for a cladding thickness of 0.1825 in. For $BP_{0.5}$ equal to the nominal operating pressure of 2.165 ksi, the *center-membrane theory* estimates a required diaphragm area of 498.9 in^2 with a cladding thickness of 0.24 in. The value of 0.24 in. is the minimum cladding thickness obtained from UT measurements of the wastage area based on a ½ inch grid.

Estimates of failure pressure with associated probabilities can be calculated for a broad range of exposed cladding areas from the theoretical treatment of circular diaphragms due to Chakrabarty and Alexander (1970) in conjunction with the stochastic model described in a previous report [1]. The thin-walled membrane assumptions applied in the theory appear to better approximate the conditions in the exposed cladding as the wastage area increases in size. It is also observed that the shape of the footprint approaches a second-order effect as the footprint area increases.

1 Introduction

1.1 Objective

In support of ongoing investigations by the United States Nuclear Regulatory Commission's (NRC) Office of Nuclear Regulatory Research, the Heavy-Section Steel Technology Program at Oak Ridge National Laboratory has carried out structural analyses of the damaged reactor pressure vessel (RPV) head located at the Davis-Besse Nuclear Power Station. This report presents the results of a finite-element analysis of the wastage area using submodeling techniques. A stochastic model, presented in an earlier report [1], is also applied to provide probabilistic estimates of the predictive uncertainty of the computational results.

1.2 Background

Pursuant to the licensee's commitments to NRC Bulletin 2001-01 [2], the Davis-Besse Nuclear Power Station began a refueling outage [3] on February 16, 2002, that included inspection of the vessel head penetrations with an emphasis on the inspection of control rod drive mechanism (CRDM) nozzles. These inspections identified axial indications in three CRDM nozzles (Nozzles 1, 2, and 3, located near the center of the RPV head) that were experiencing pressure-boundary leakage. Upon completing boric acid removal on March 7, 2002, the licensee conducted a visual examination of the area and identified a large cavity in the RPV head on the downhill side of CRDM Nozzle 3. Followup characterization by ultrasonic testing (UT) indicated wastage of the low alloy steel RPV head material adjacent to the nozzle. The wastage area was found to extend approximately 5 inches downhill on the RPV head from the penetration for CRDM Nozzle 3, with a width of approximately 4 to 5 inches at its widest part.

See Fig. 1. for a photograph of the Davis-Besse RPV, a schematic of a typical nuclear power reactor showing the location of the CRDM nozzles relative to the RPV, and a sketch and photographs of the cavity and wastage area around Nozzle 3.

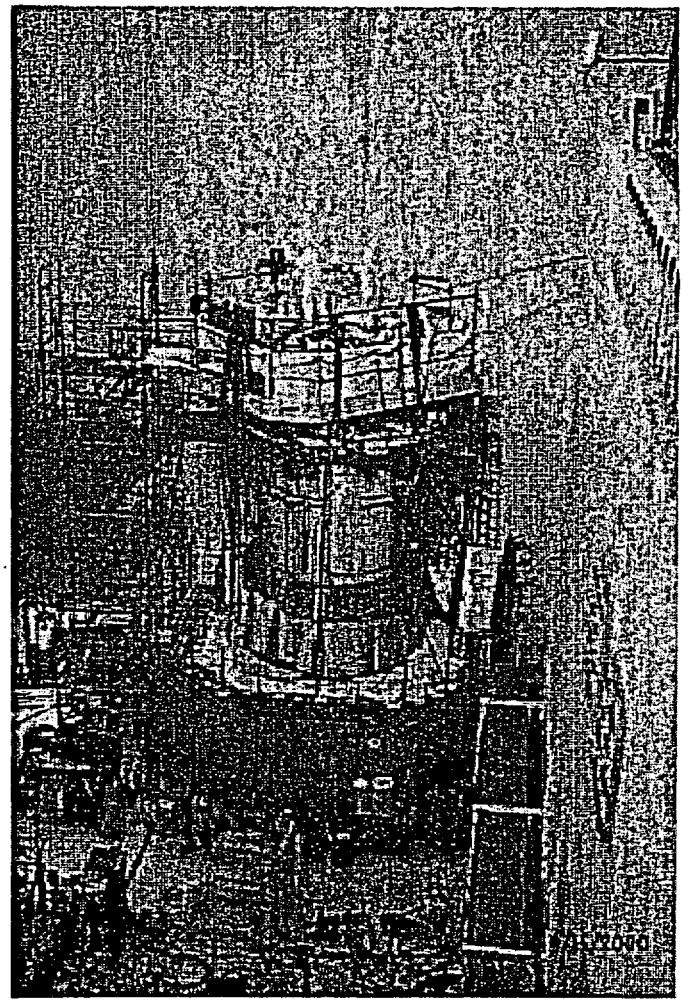

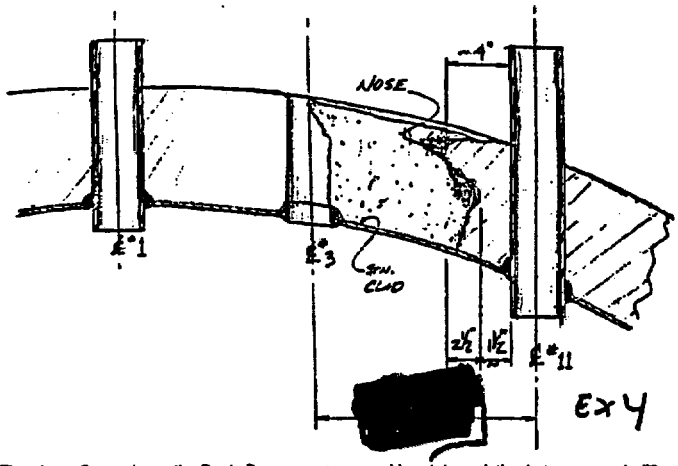

The above figure shows the Davis Besse reactor vessel head degradation between nozzle #3 and nozzle #11. This sketch was provided to the NRC by the Licensee.

Fig. 1. (a) Davis-Besse Nuclear Power Station RPV and (b) sketch of RPV head degradation.

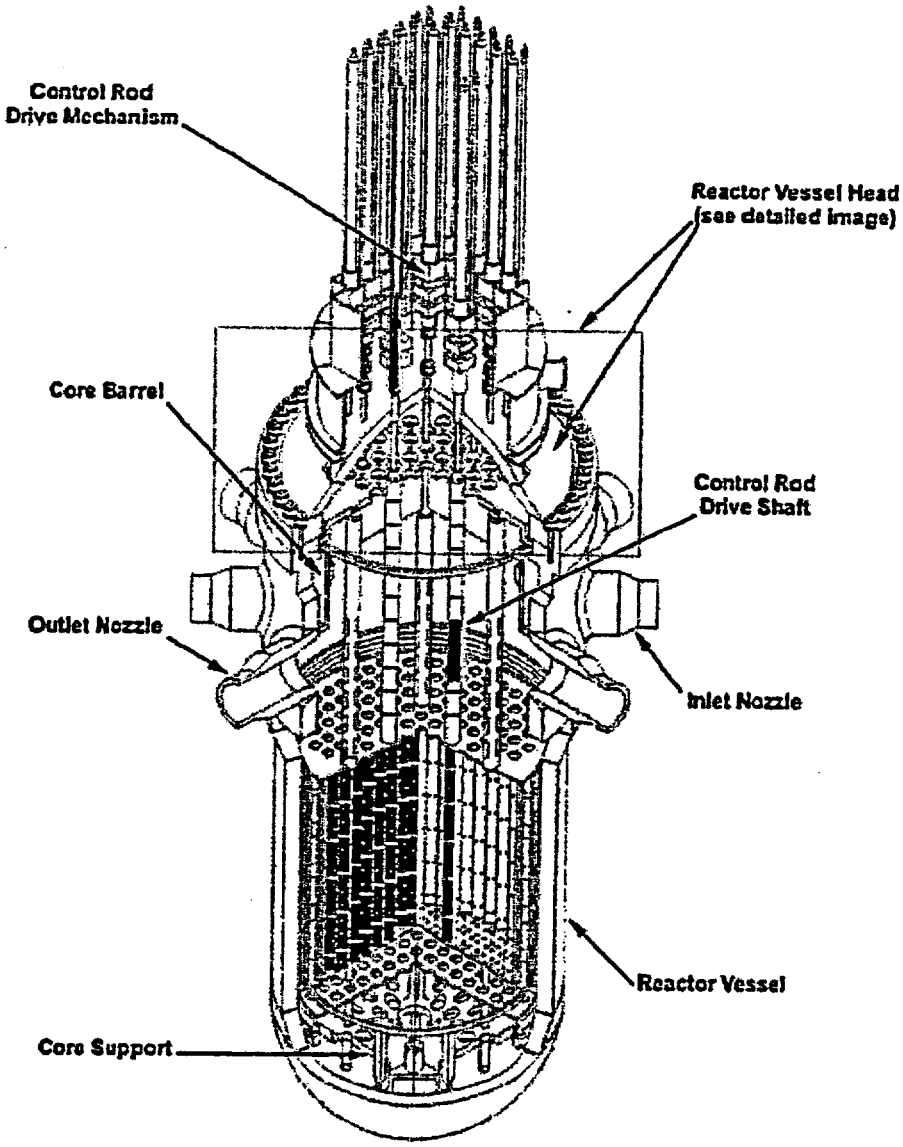

Fig. 1 (continued) (c) schematic of a typical nuclear power reactor showing the relationship of the CRDM nozzles to the RPV head.

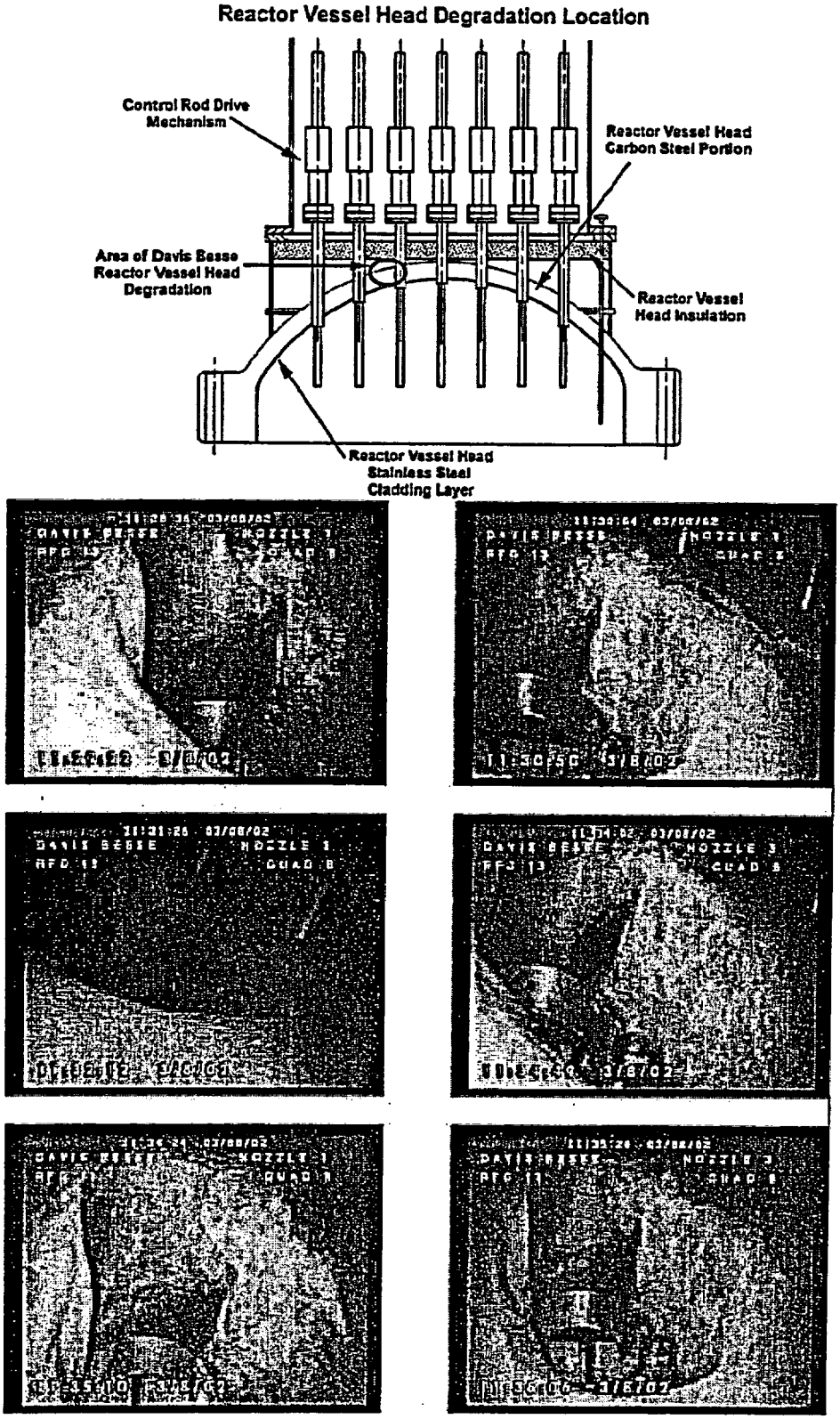

Fig. 1. (continued) (d) photographs of the wastage area and cavity with Nozzle 3 removed.

1.3 Scope

Section 2 reviews the geometry and material properties used in the development of the finite-element global and submodels; Section 3 presents the algorithms used to estimate the growth patterns of the wastage-area footprint; Section 4 presents the results of both the bounding calculations for the "as found" condition of the wastage area and the growth-pattern results compared to the predictions of a theoretical treatment of failure in circular diaphragms; and Section 5 provides a summary and conclusions.

2 Geometry and Material Properties

2.1 "As-Found" Footprint Geometry

Tables 1 and 2 present the details of the "as-found" geometry of the wastage area. The figure in Table 2 was taken from Fig. 13 of the *Root Cause Analysis Report, Significant Degradation of Reactor Pressure Vessel Head,* CR 2002-0891 [4]. The "as-found" footprint in Table 2 was digitized with CorelDraw 10®. Additional details for the "as-found" case are given in [1].

2.2 Material Properties

Three materials are used in the construction of the finite-element submodel of the wastage area: (1) Alloy 600 for the CRDM tubes, (2) A533B for the base material of the vessel, and (3) SS308 for the subarc weld (SAW) cladding. Elastic properties [5] for these three materials are shown in Fig. 2 as a function of temperature. Figure 3 presents plastic properties [5] (effective stress as a function of effective plastic strain) for Alloy 600 and A533B pressure vessel steel. An adjusted SS308 stress vs. strain curve used in the bounding-case calculations is compared in Fig. 4 to curves from a range of A8W heats (SS304 pipe with SS308 weld from the PIFRAC database [5]) and the unadjusted stress vs. strain curve received from Framatome [6]. Strain hardening for the adjusted curve was reduced to lower-bound all of the data, where the offset yield strength and strain at ultimate strength were retained from the unadjusted SS308 curve. This adjusted stress/strain curve was applied in the "bounding" calculation for the "as-found" condition and all subsequent cavity growth cases.

2.3 Finite-Element Global and Submodels of Wastage Area and Cavity

The submodeling capabilities of the ABAQUS finite-element code [7] were employed in this analysis to focus the available computational resources on the region of interest located around the wastage area cavity at CRDM Nozzle 3. Submodeling can be used to investigate a portion of a model with a refined mesh. The boundary conditions of the *submodel* are driven by an interpolation of the displacement solution from an initial, relatively coarse, *global model.* The technique is primarily useful when it is necessary to obtain a refined, detailed solution in a local region, and the detailed modeling of that local region has a negligible effect on the global solution, i.e., solution information is passed in one direction only, from the global model to the submodel.

As shown in Figs. 5a and 6, the global model consists of the full RPV head (with all 69 penetrations) and closure flange. No cladding or CRDM nozzles are included in the global model. The submodel (see Fig. 5b) consists of the cladding (SS308), base (A533B), and CRDM Nozzles (A600) 3, 11, 15, and 16. The plan views of the RPV head in Fig. 7a and 7b indicate the position and geometry of the submodel

with respect to the global model. Figure 8 shows the ProEngineer® solid model of the submodel. This solid model was imported into MSC Patran® where the finite-element mesh was constructed.

Table 1. Wastage-Area-Footprint Geometry Data

Description	Scaling Factor	Area	Perimeter	Centroid of Wastage Area Footprint		Moments of Inertia About the Centroid			Eigenvalue Extraction for Principal Moments and Directions			
									Principal Moments		Principal Directions	
		(in^2)	(in.)	(in.)	(in.)	(in^4)	(in^4)	(in^4)	(in^4)	(in^4)	I_1	I_2
As-Found Footprint	1	35.36	30.36	16.4122	-0.1194	98.89	9699.33	-117.16	75.26	197.41	<0.9004, -0.4351>	<0.4351, 0.9004>
Adjusted Footprint for Bounding Calculation	0.25 in.	40.06	31.78	16.4301	-0.1255	129.02	11031.81	-141.35	99.00	245.71	<0.8943, -0.4476>	<0.4476, 0.8943>

Footprint centroid is in global coordinates.
Global coordinate system has its z-axis aligned with the vertical centerline of the vessel.
The x-y plane of the global coordinate system is a horizontal plane
with the x-axis along the line between the centerlines of Nozzles 3 and 11.

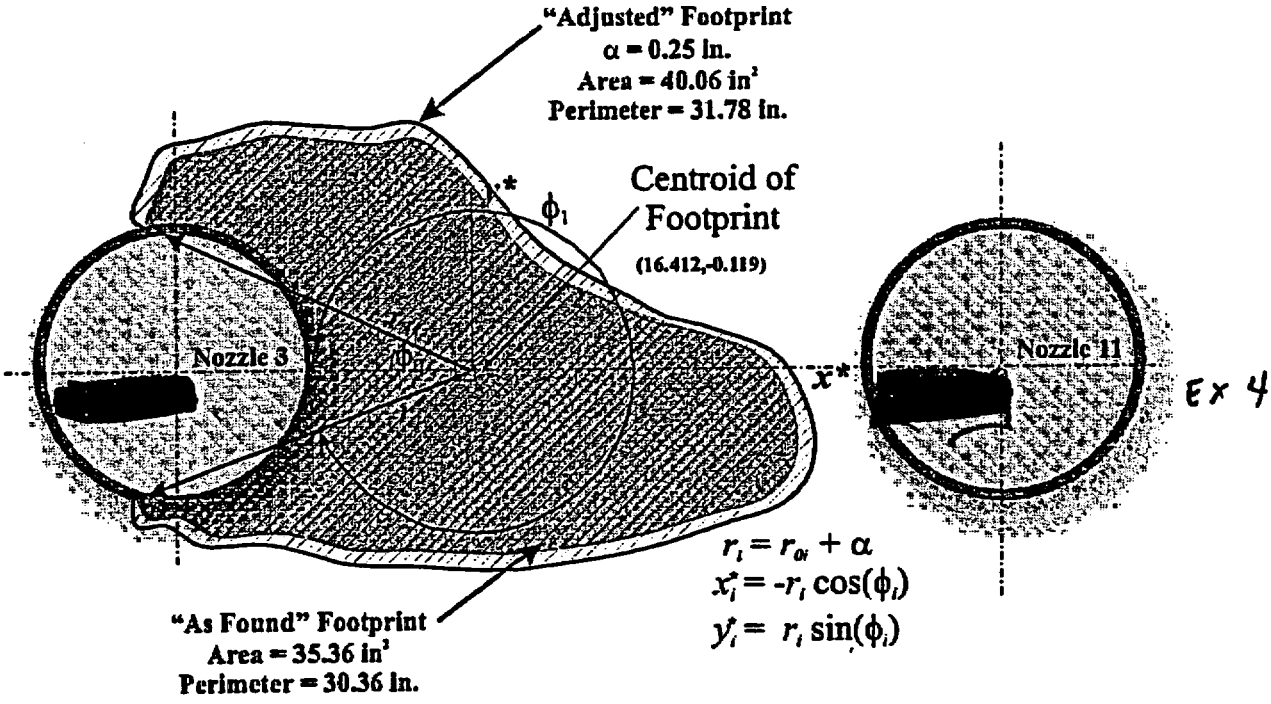

EX 4 EX 4

2.4 Loading and Constraint Conditions

Only mechanical loading due to the internal pressure of the coolant was considered in these analyses. The pressure load was applied to the inner surface of the vessel and the inside of the CRDM nozzles. Tied contact constraints were established between the cladding and base material interface and between the CRDM nozzles and the cladding and base. The J-groove weld attaching the nozzle to the vessel was not explicitly modeled. The vertical surfaces of the submodel were driven by the interpolated displacement solution obtained with the global model of the RPV head (see Fig. 5).

Table 2. Details of Wastage Area Footprint Before Adjustment for Bounding Calculation (Figure taken from Fig. 13 ref. [4])

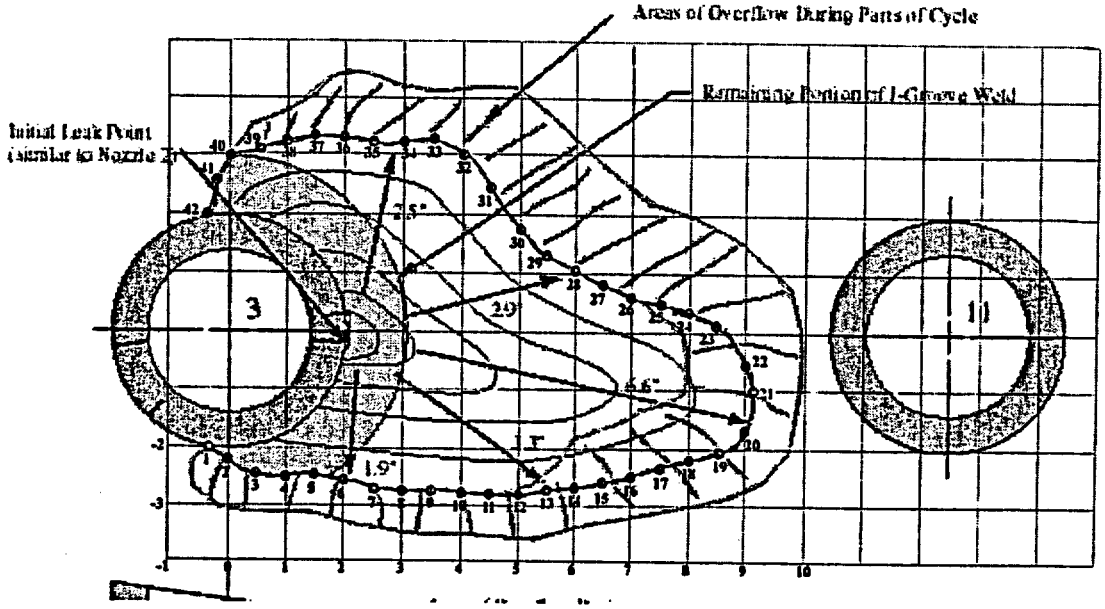

Point	x'	y'	Point	x'	y'
0	-0.639	-1.895	24	8.000	0.334
1	-0.334	-2.280	25	7.500	0.483
2	0.000	-2.235	26	7.000	0.582
3	0.500	-2.492	27	6.500	0.829
4	1.000	-2.522	28	6.000	1.046
5	1.500	-2.482	29	5.500	1.303
6	2.000	-2.581	30	5.000	1.778
7	2.500	-2.730	31	4.500	2.460
8	3.000	-2.769	32	4.000	3.023
9	3.500	-2.759	33	3.500	3.300
10	4.000	-2.789	34	3.000	3.221
11	4.500	-2.819	35	2.500	3.250
12	5.000	-2.819	36	2.000	3.300
13	5.500	-2.759	37	1.500	3.349
14	6.000	-2.700	38	1.000	3.240
15	6.500	-2.621	39	0.500	3.122
16	7.000	-2.512	40	0.000	3.000
17	7.500	-2.364	41	-0.210	2.578
18	8.000	-2.216	42	-0.364	2.000
19	8.500	-2.087	43	-0.242	1.985
20	9.000	-1.712			
21	9.135	-1.000			
22	9.000	-0.555			
23	8.500	0.137			

Origin of local coordinate system located at centerline of Nozzle 3. (inches)

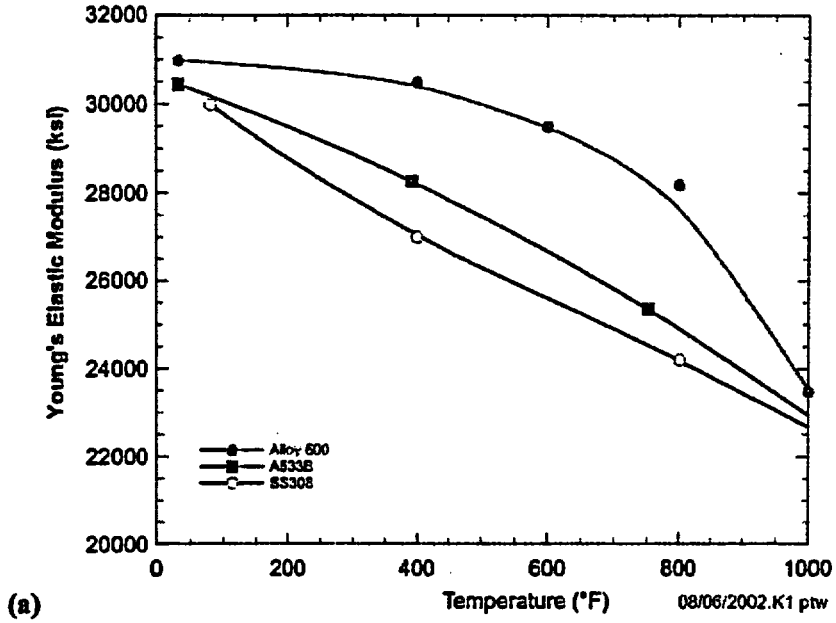

(a)

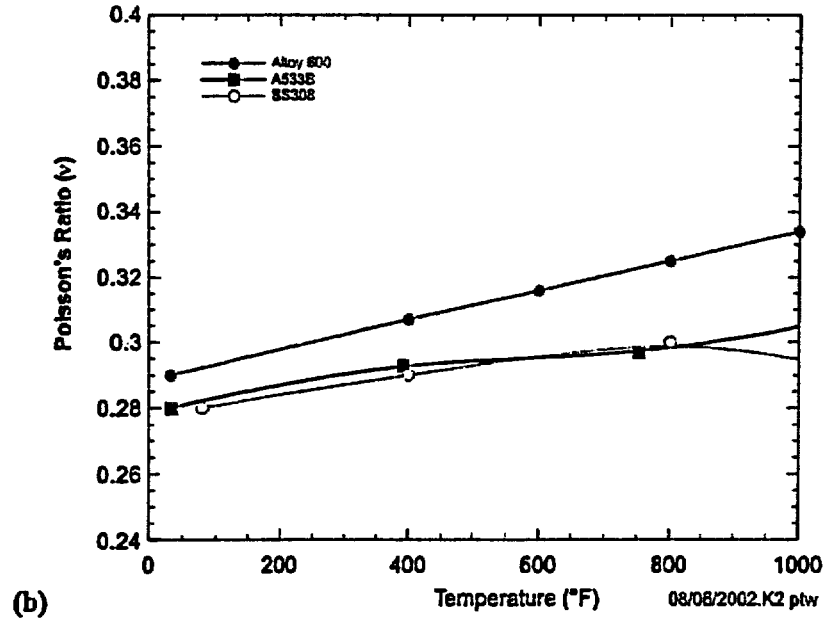

(b)

Fig. 2. Elastic properties [5] of the materials used in the finite-element models of the wastage area: (a) Young's elastic modulus and (b) Poisson's ratio.

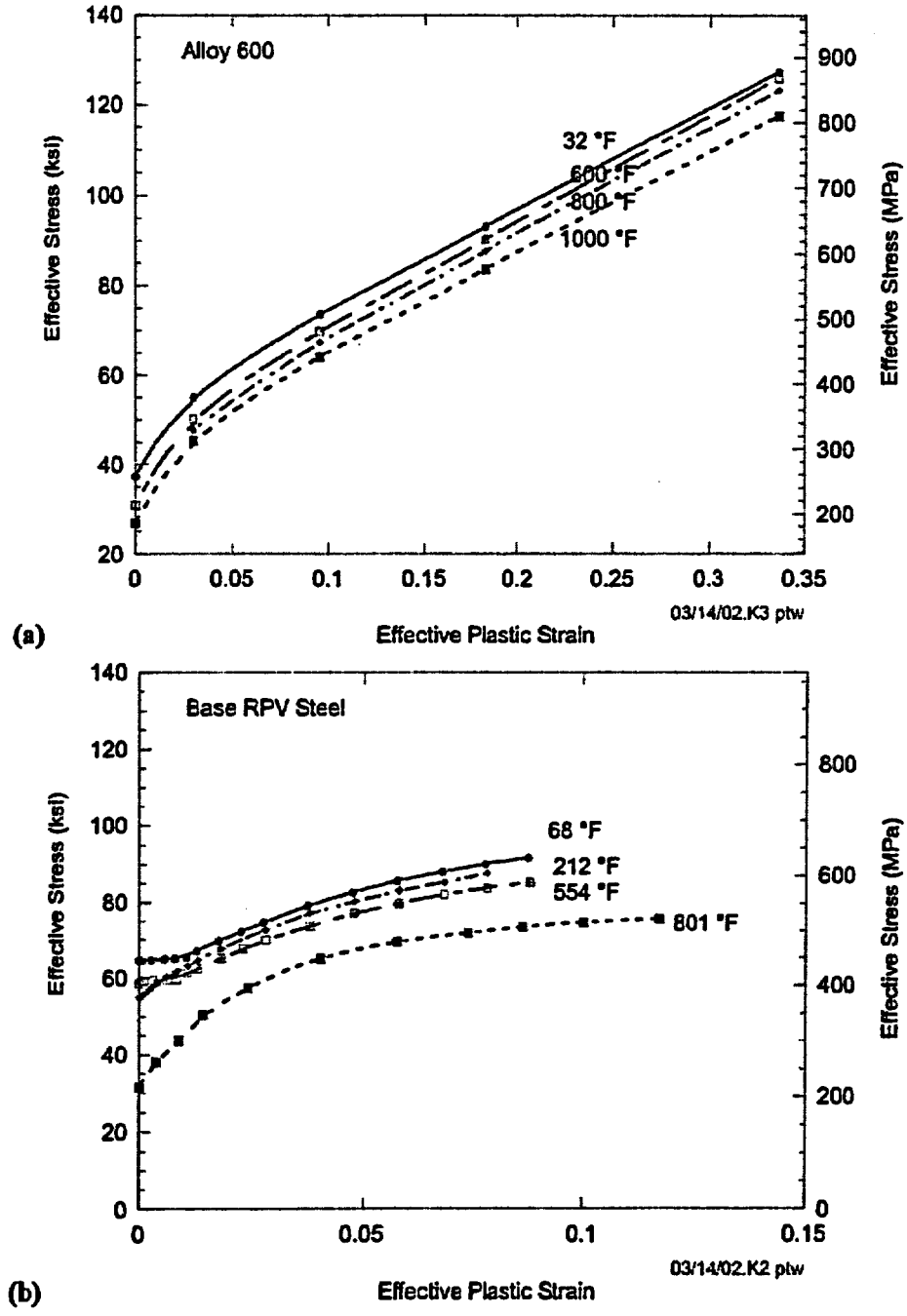

Fig. 3. Plastic property data [5] used in global and submodel: (a) Alloy 600 and (b) A533B pressure vessel steel.

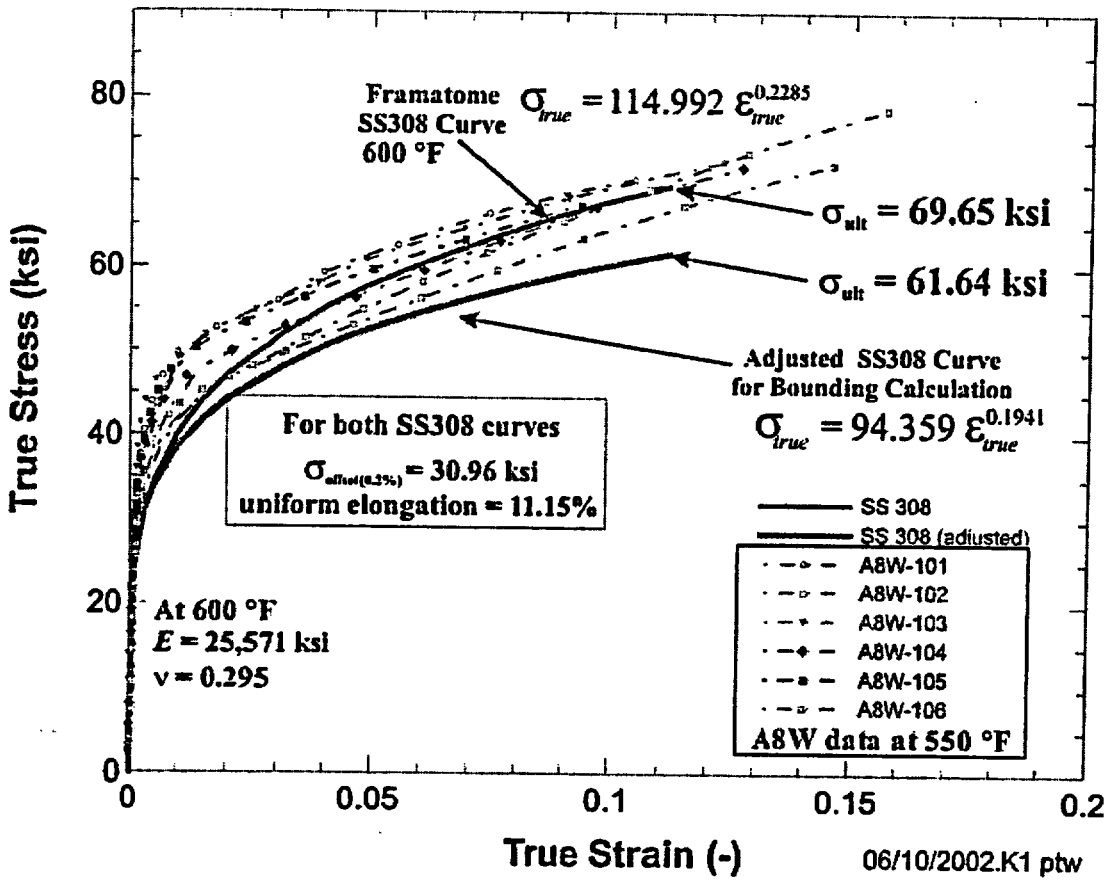

Fig. 4. Adjusted SS308 stress vs. strain curve used in the bounding-case calculations compared to curves from a range of A8W heats [5]. Strain hardening in the adjusted curve was reduced to lower-bound all of the data. The offset yield strength and strain at ultimate strength were retained from the unadjusted SS308 curve received from Framatome [6].

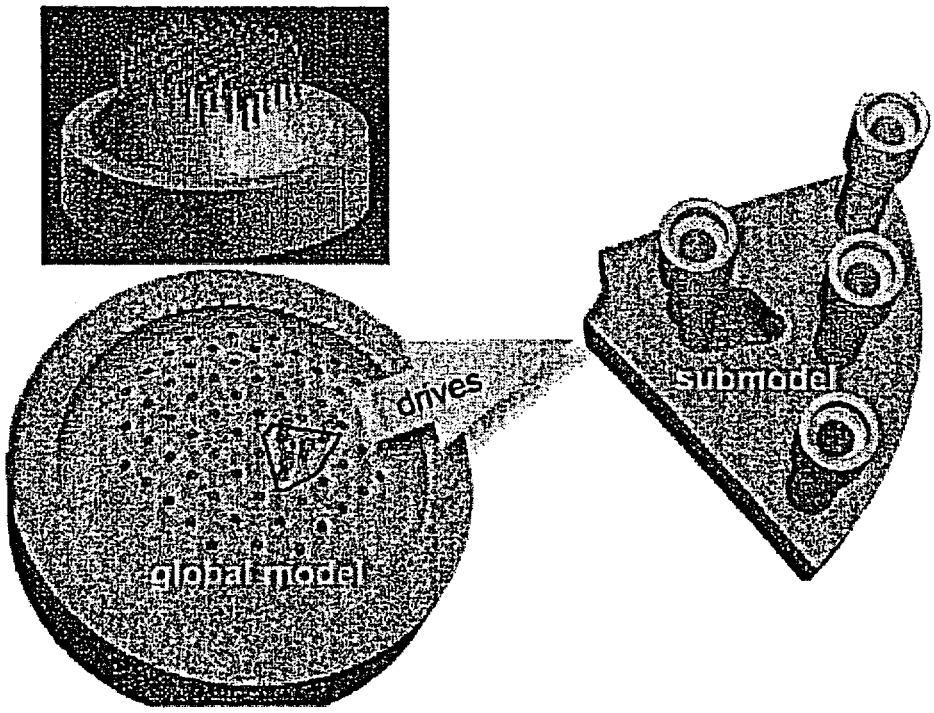

(a)

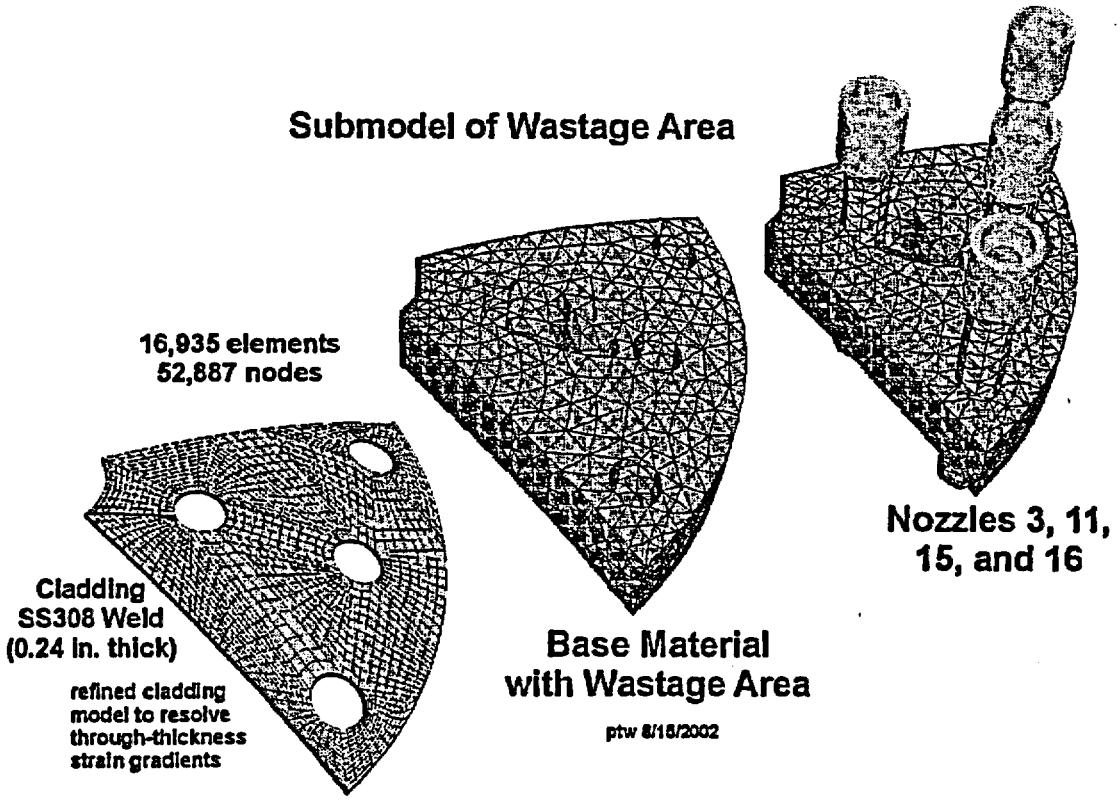

(b)

Fig. 5. Finite-element global and submodels of the Davis-Besse head and wastage area. The displacements at the vertical side boundaries of the submodel are driven by the global model. Both models are exposed to the same internal pressure loading.

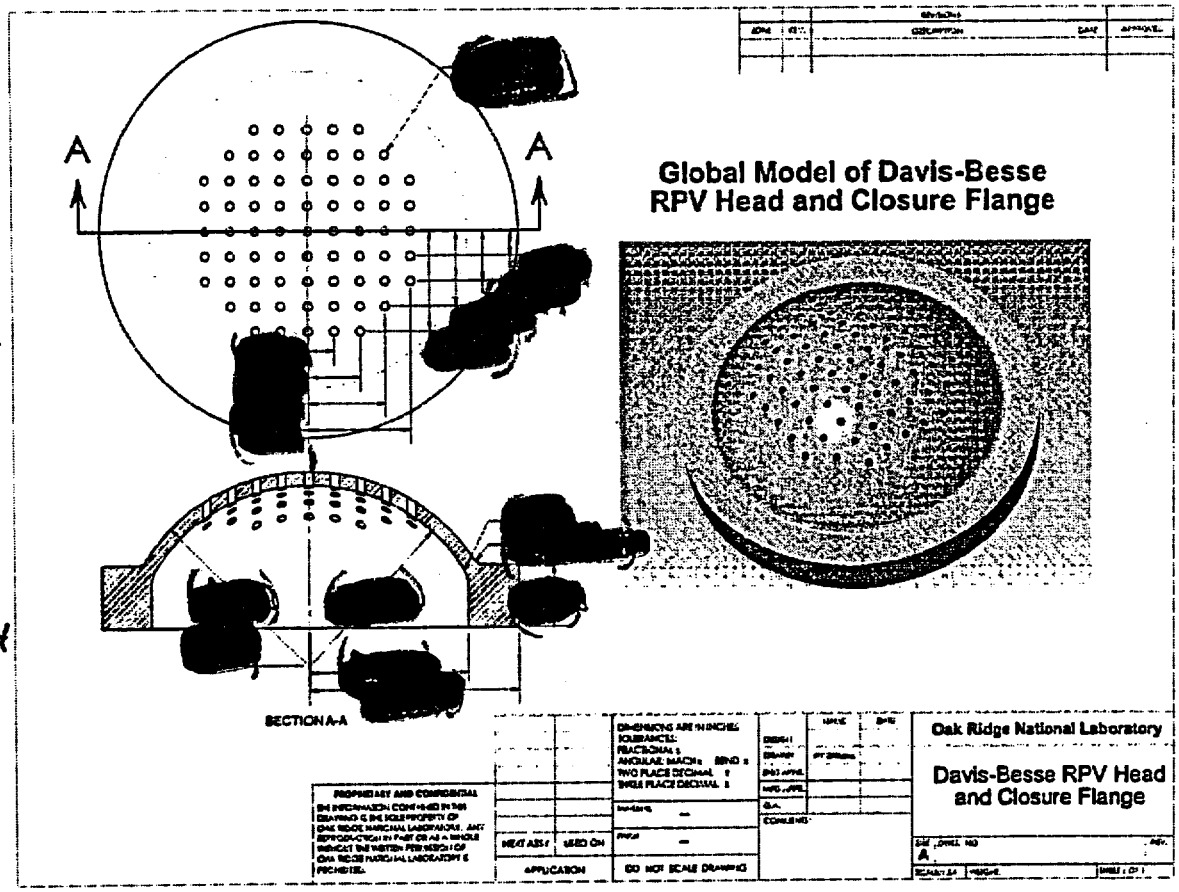

Ex 4

Ex 4

Fig. 6. Geometry of RPV head and closure flange used in global model.

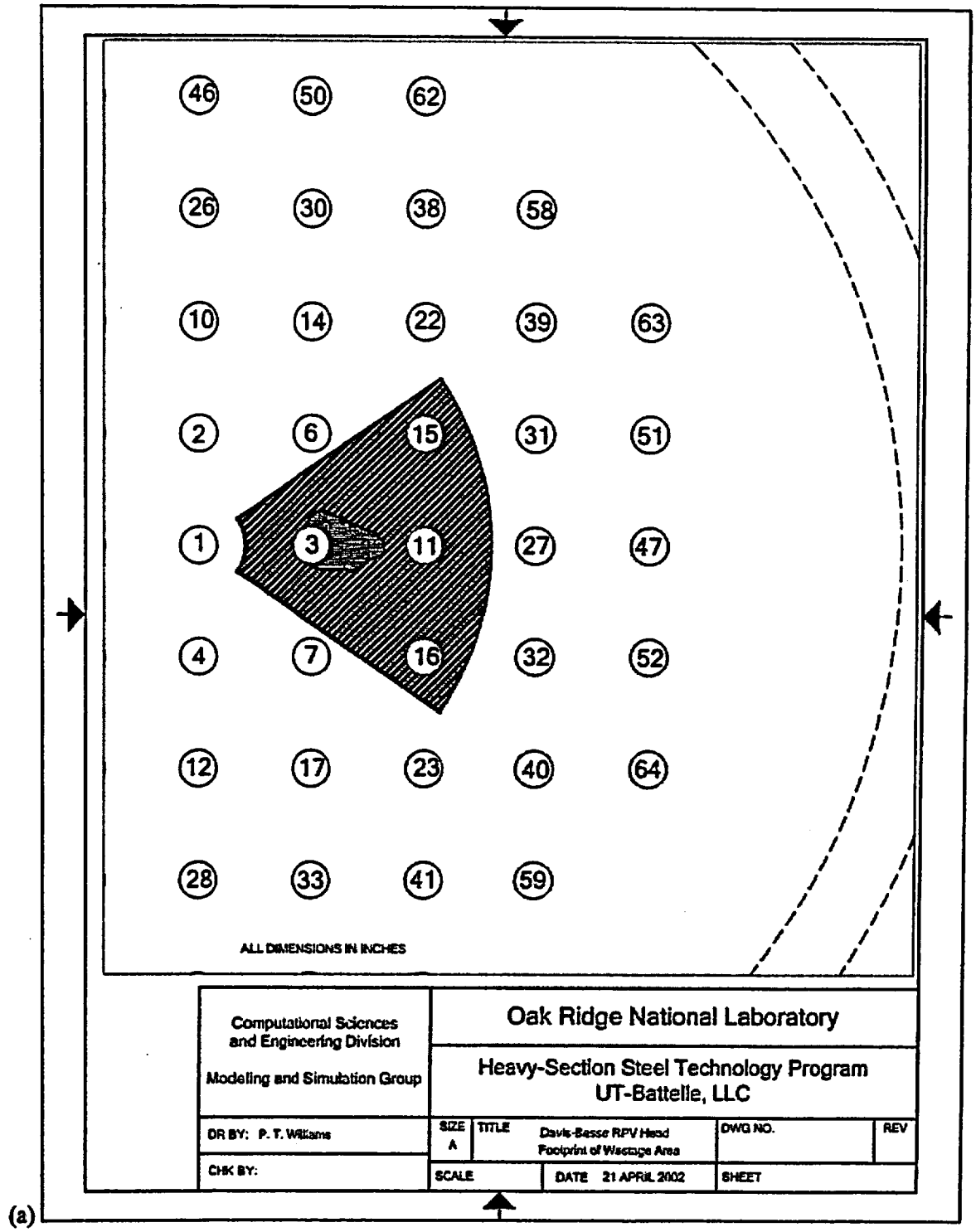

Fig 7. (a) Relative location of submodel within full RPV head,

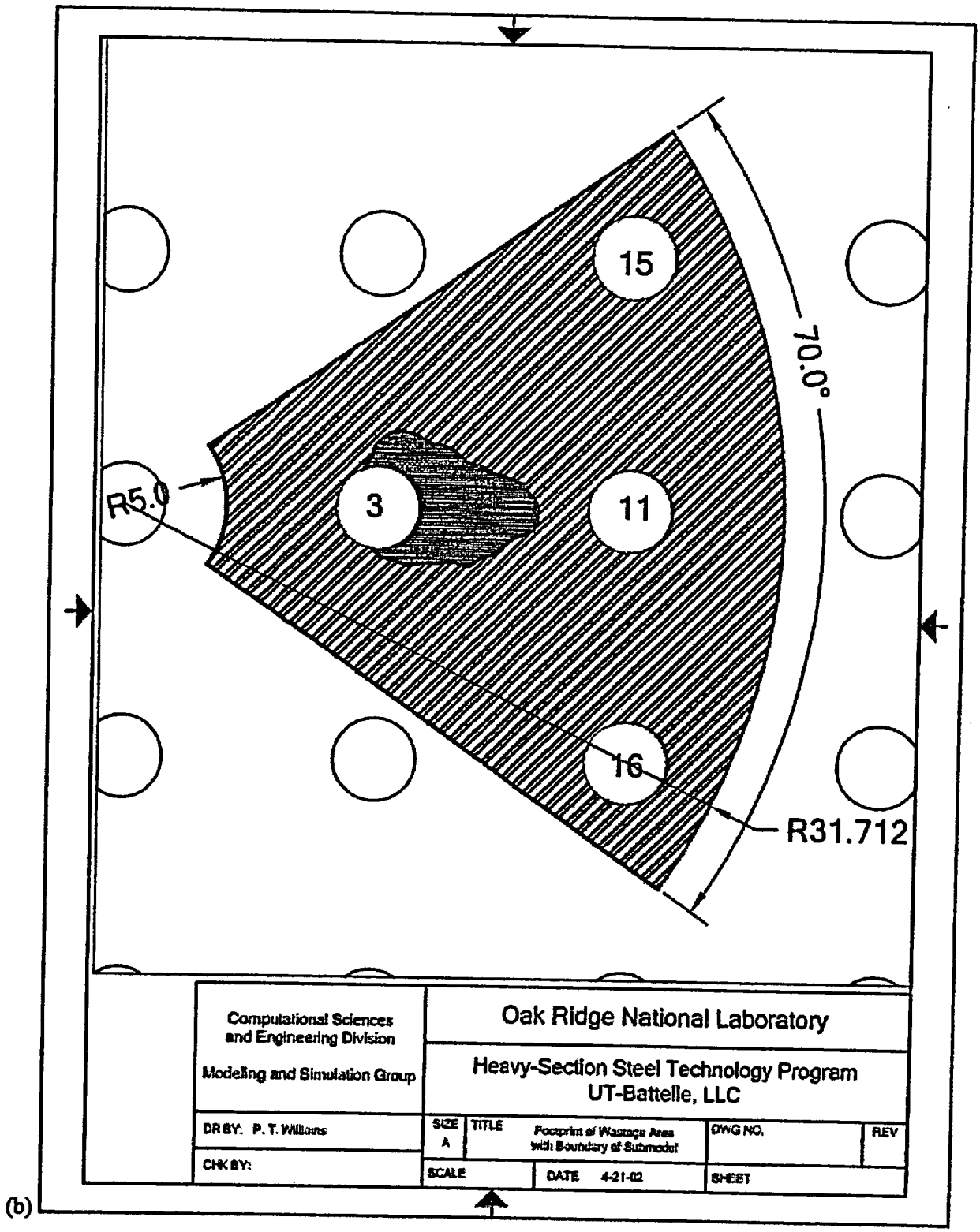

Fig. 7. (continued) (b) geometry of submodel relative to Nozzles 3, 11, 15, and 16.

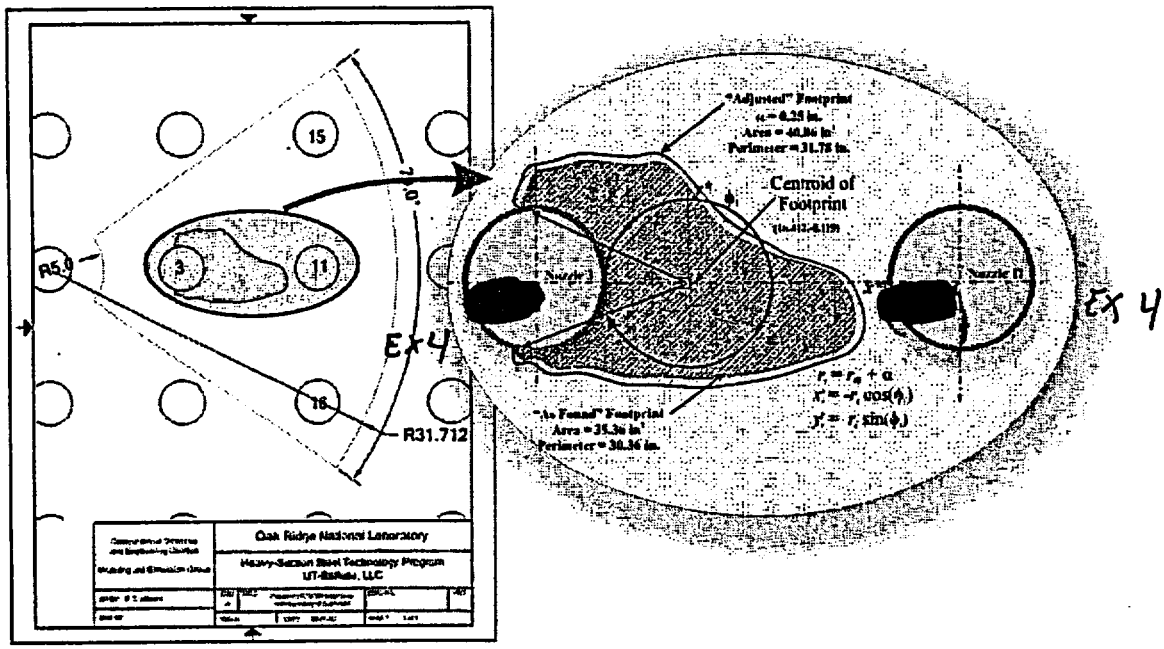

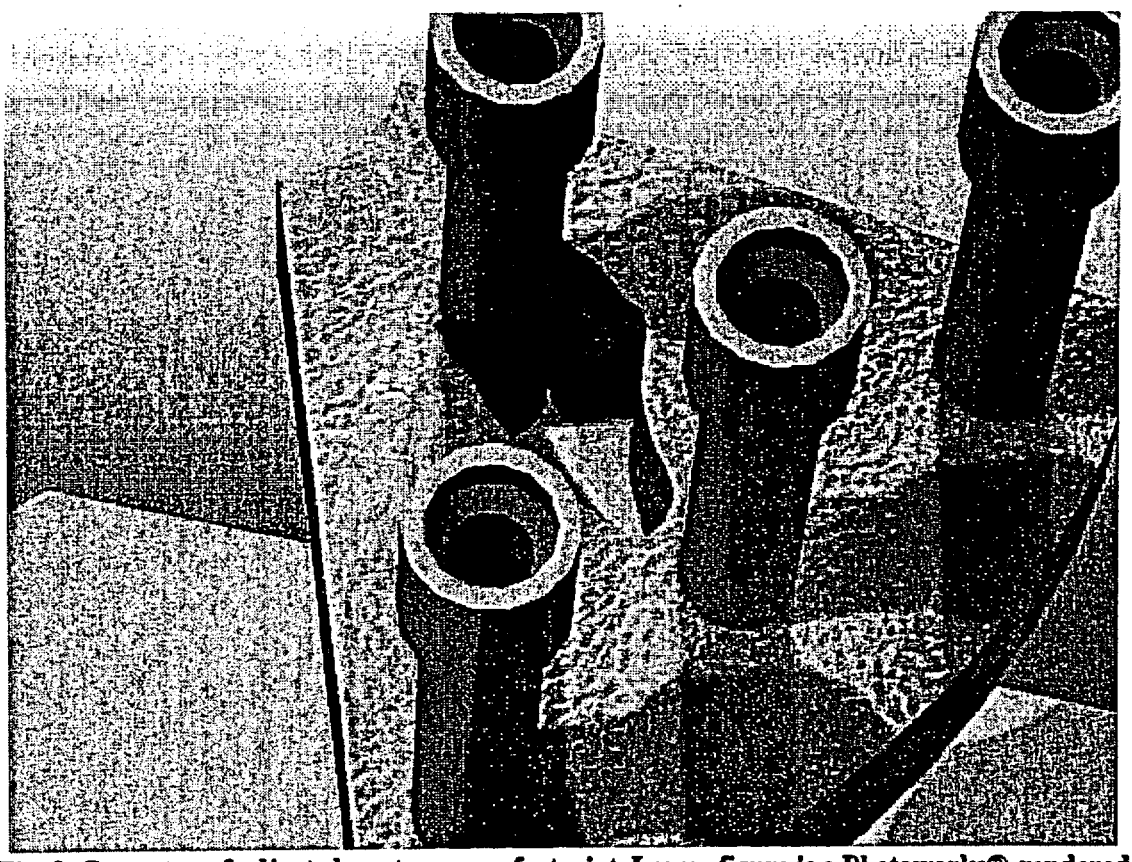

Fig. 8. Geometry of adjusted wastage area footprint. Lower figure is a Photoworks®-rendered image of the submodel with the adjusted "as-found" footprint.

3 Postulated Growth Patterns

3.1 *Self-Similar* Growth Pattern

The *self-similar* growth-pattern scheme attempts to maintain, as closely as practicable, the general shape of the "as-found" cavity footprint. New growth footprints are scaled from a local coordinate system with its origin positioned at the centroid of the "as-found" footprint. A position vector, $\overline{r_0}$, tracks the profile of the footprint using the polar coordinates (r_i, ϕ_i) at the 44 points defined in Table 2. At each point along the footprint, the magnitude of the position vector is increased by a constant scaling factor, α, and then mapped back to the local rectangular Cartesian coordinate system by the following algorithm

$$\begin{aligned} &\text{for } i = 0,43 \\ &\quad r_{0i} = \sqrt{x_{0i}^2 + y_{0i}^2} \\ &\quad r_i = \alpha \times r_{0i} \\ &\quad x_i = -r_i \cos(\phi_i) \\ &\quad y_i = r_i \sin(\phi_i) \end{aligned} \tag{1}$$

as shown in Fig. 9. This local coordinate system is subsequently mapped to the coordinate system used in the ABAQUS global model and submodels. Figure 10 shows the five growth patterns investigated for $\alpha = \{1.6, 2.0, 2.8, 3.0, 3.4\}$. The scaled footprint's centroid, perimeter, area, and higher moments were calculated with AutoCad 2002 by converting a closed spline to a region and then applying AutoCad's *Region Mass Properties* utility. These footprint details are given in Table 3. The exposed-cladding surface area ranged from 86 to 276 in^2. Four of the five growth patterns (as indicated in Fig. 10) intercepted and were constrained by the outer boundaries of the submodel. A second growth-pattern scheme was developed to check the sensitivity of the results to this interaction with the submodel boundaries.

3.2 *Ellipsoidal* Growth Pattern

In Fig. 11, the *ellipsoidal* growth-pattern scheme established a partially elliptical or ovalized footprint extending between Nozzles 3 and 11. The growth is parameterized by the variable δ which serves as the transverse (initially minor) axis footprint extending between the two nozzles. The longitudinal (initially major) axis also varies. The exposed-cladding surface area ranges from 99 to 254 in^2 for the ellipsoidal growth patterns.

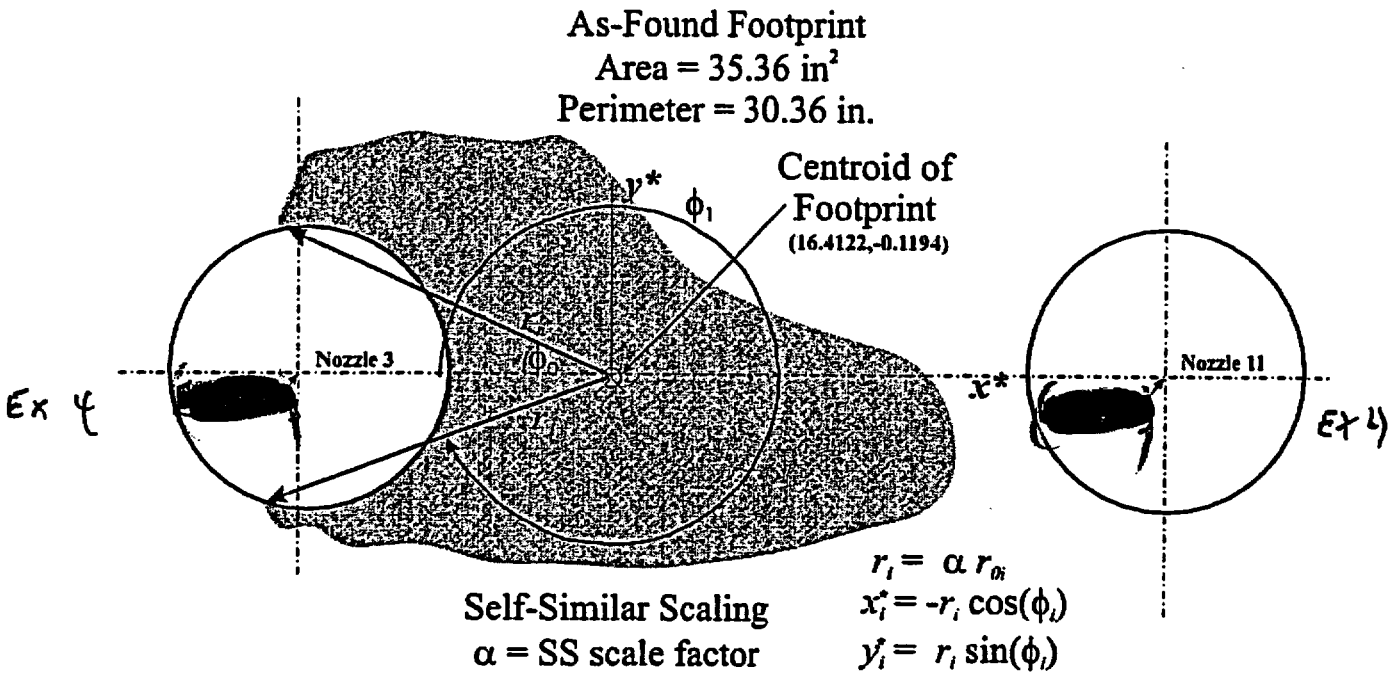

Fig. 9. Local coordinate system employed in *self-similar* growth patterns with scaling of footprint based on scale factor, α.

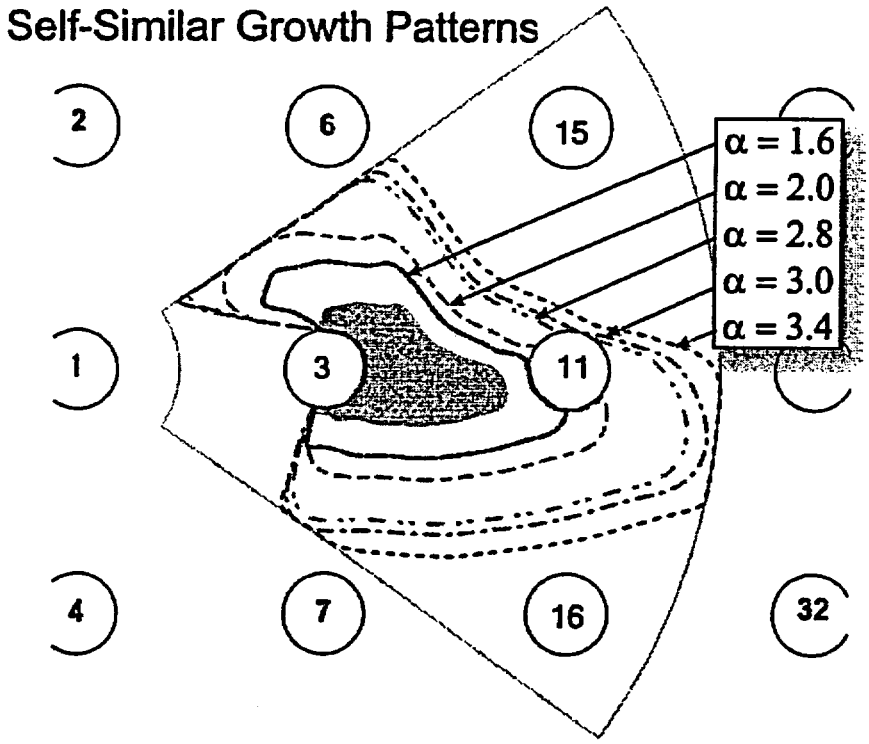

Fig. 10. Expansion of self-similar growth patterns constrained at submodel boundaries.

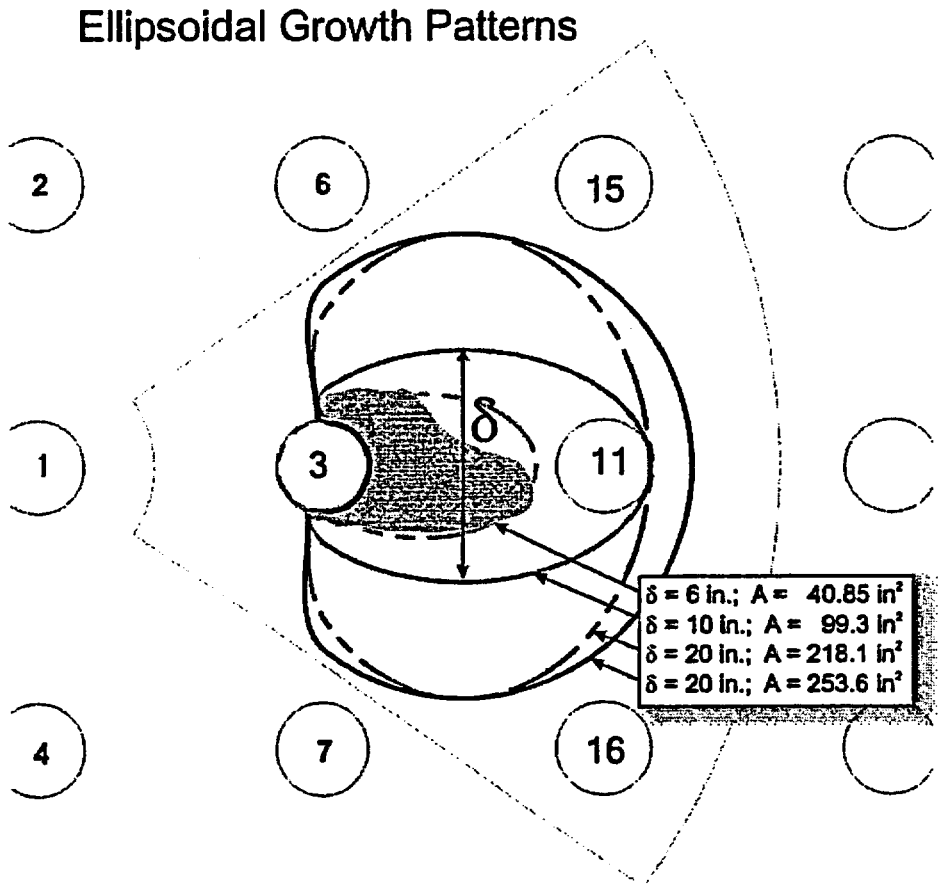

Fig. 11. All *ellipsoidal* growth patterns contained within submodel boundaries.

4 Results and Discussion

Table 3 presents the results of cavity-growth calculations using the ABAQUS finite-element submodels of postulated wastage areas for the two growth pattern schemes described in Sect. 3. The pressures calculated at numerical instability are compared in Fig. 12a to burst pressures for circular diaphragms estimated by the critical-strain theory of Chakrabarty and Alexander [8]. The finite-element analyses applied a nonlinear finite-strain procedure with an incremental pressure load increasing from zero up to the load at which numerical instabilities caused ABAQUS to abort the execution. The internal pressure attained immediately preceding the onset of numerical instability was designated in [1] as the *pressure at numerical instability*, P_{NI}. This calculated pressure is linked to an estimated failure pressure with an associated probability through the application of a stochastic model developed in [1].

The theoretical treatment of critical strains in circular diaphragms under lateral pressure loading is discussed in refs. [1, 8, and 9]. In summary, the application of the theory to the wastage-area problem proceeds as follows:

- Calculate the effective critical strain [8]. $\bar{\varepsilon}_{crit} = \dfrac{2(2-n)(1+2n)}{11-4n}$
- Calculate the corresponding effective critical stress. $\bar{\sigma}_{crit} = K\,\bar{\varepsilon}^{n}$
- Calculate the critical thickness. $h_{crit} = h_0 \exp(-\bar{\varepsilon}_{crit})$
- Calculate the polar height at the critical-strain. $H_{crit} = a\sqrt{\exp\left(\dfrac{\bar{\varepsilon}_{crit}}{2}\right)-1}$
- Calculate the corresponding bulge curvature radius. $R_{crit} = \dfrac{H_{crit}^2 + a^2}{2H_{crit}}$
- Finally, calculate the predicted diaphragm burst pressure. $p_{burst} = \dfrac{2h_{crit}\bar{\sigma}_{crit}}{R_{crit}}$

From the SS308 properties of the bounding case with a clad thickness of 0.24 in. and the geometry of Fig. 13, the following variables are set

$$n = 0.1941 \qquad h_0 = 0.24 \text{ in.}$$
$$K = 94.359 \text{ ksi} \quad a = (Area/\pi)^{1/2} \text{ in.}$$

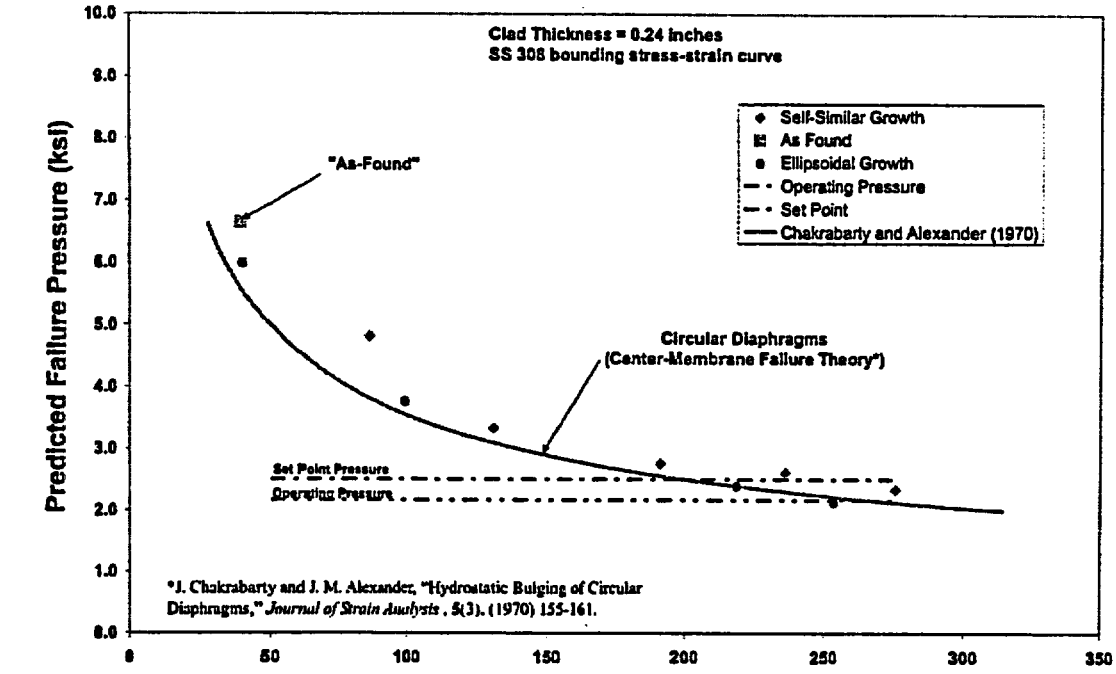

(a)

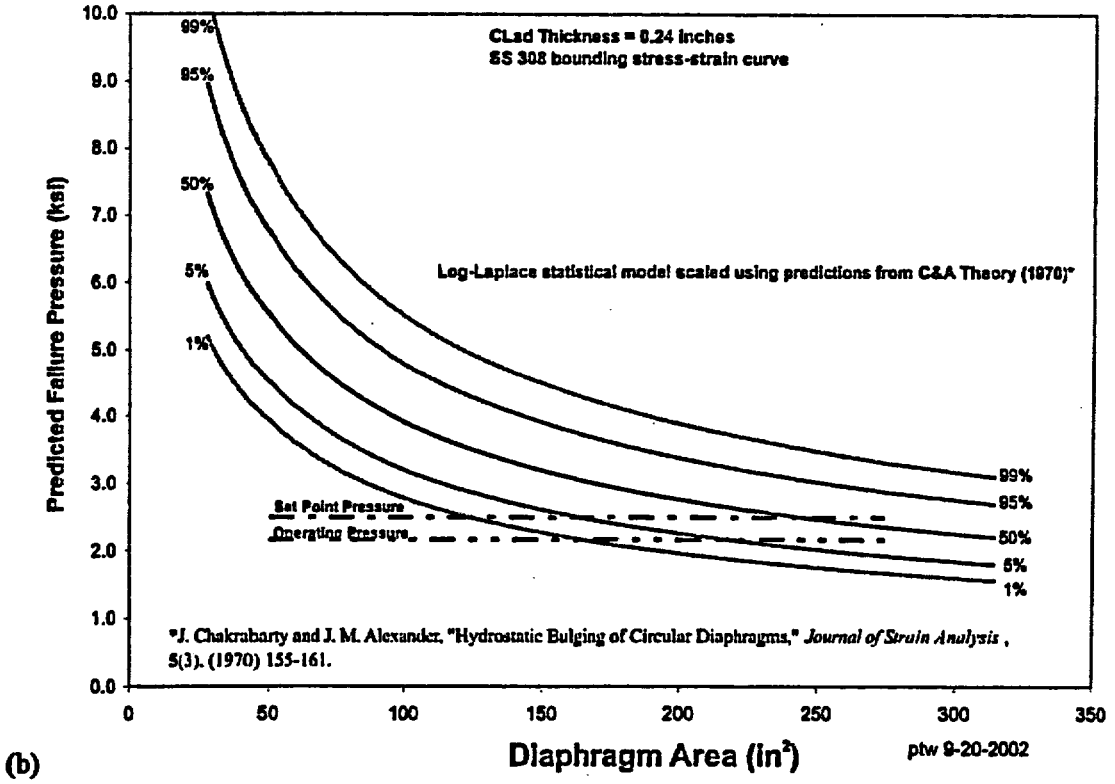

(b)

Fig. 12. Failure pressures as a function of footprint area: (a) pressures at numerical instability, P_{NI}, calculated by ABAQUS finite-element submodels of postulated footprints are compared to burst pressures in circular diaphragms predicted by the theory of Chakrabarty and Alexander (1970) and (b) stochastic failure model scaled from the theory of Chakrabarty and Alexander (1970).

In general, the finite-element P_{NI} predictions in Fig. 12a can be observed to follow the trends predicted by the theory of Chakrabarty and Alexander [8] when the exposed-cladding footprint area serves as the primary independent variable. As the exposed-cladding area increases, the agreement between computational and theoretical predictions improves. This improvement may be in part due to the increasing validity of the "thin-walled membrane" assumptions applied in the theoretical model.

The theoretical model assumes that the critical strain occurs at the maximum polar height of the spherically-deforming membrane. Edge effects in the diaphragm are not considered, and the theory focuses on failure at the center of circular diaphragm only. From inspection of the plastic strain contour plots near failure in the finite-element models, it was observed that the maximum plastic strains occurred along the edges of the footprint, thus indicating a higher probability of edge failures rather than center failures. One explanation for the good agreement between the center-membrane failure theory and the computational results may be that, even though failures may be more likely to occur first at the edges of the footprint, as the area increases failure within the interior of the footprint (as predicted by the theory) may also be imminent.

Table 3. Case Matrix and Failure Pressure Results

Description	Scaling Parameter	Pressure at Numerical Instability	Failure Pressures at Selected Probabilities			Cladding Thickness	Footprint Area	Footprint Perimeter	Footprint Centroid		Moments of Inertia About Centroid		
			5%	50%	95%				x_c	y_c	I_{xx}	I_{yy}	I_{xy}
		(ksi)	0.05	0.5	0.95	(in.)	(in^2)	(in.)	(in.)	(in.)	(in^4)	(in^4)	(in^4)
As-Found Footprint	1						35.36	30.36	16.4122	-0.1194	98.9	9699.3	-117.2
Adjusted Footprint for Bounding Calculation	additive +0.25 in.	6.65 5.18	6.01 4.68	7.35 5.73	8.99 7.00	0.24 0.1825	40.06 40.06	31.78 31.78	16.4301 16.4301	-0.1255 -0.1255	129.0 129.0	11031.8 11031.8	-141.3 -141.3
	α												
Self-similar	1.6	4.82	4.36	5.33	6.52	0.24	86.04	50.09	16.1199	-0.0503	659.4	23404.4	-395.0
Self-similar	2.0	3.33	3.01	3.68	4.50	0.24	130.95	65.19	15.8900	-0.0450	1593.8	35503.8	-882.4
Self-similar	2.8	2.75	2.49	3.04	3.72	0.24	191.37	79.54	18.0980	-0.5830	4017.2	72416.6	-4117.5
Self-similar	3.0	2.60	2.35	2.87	3.51	0.24	235.80	76.60	18.5550	-0.7060	4979.9	93748.1	-5599.1
Self-similar	3.4	2.33	2.11	2.58	3.15	0.24	276.28	80.86	19.2100	-1.0140	6840.7	116863.9	-8425.6
	δ (in.)												
Ellipsoidal	10	3.76	3.40	4.16	5.08	0.24	99.32	43.28	18.9810	-0.0090	766.3	41716.2	-12.0
Ellipsoidal	20	2.40	2.17	2.65	3.24	0.24	218.06	59.02	18.7660	-0.0170	6158.1	84305.8	-45.1
Ellipsoidal	20a	2.14	1.94	2.37	2.89	0.24	253.65	63.26	19.3330	-0.0190	7302.3	104200.3	-59.7
Ellipsoidal	20a*	2.18	1.97	2.41	2.93	0.24	253.65	63.26	19.3330	-0.0190	7302.3	104200.3	-59.7
Ellipsoidal	6.2	5.99	5.42	6.62	8.10	0.24	40.85	28.1	15.9500	0	123.1	14013.5	-0.3

*Same as previsous case, except Nozzle 11 constrained from vertical displacement.

Footprint centroid is in global coordinates.
Global coordinate system has its z-axis aligned with the vertical centerline of the vessel.
The x-y plane of the global coordinate system is a horizontal plane
with the x-axis along the line between the centerlines of Nozzles 3 and 11.

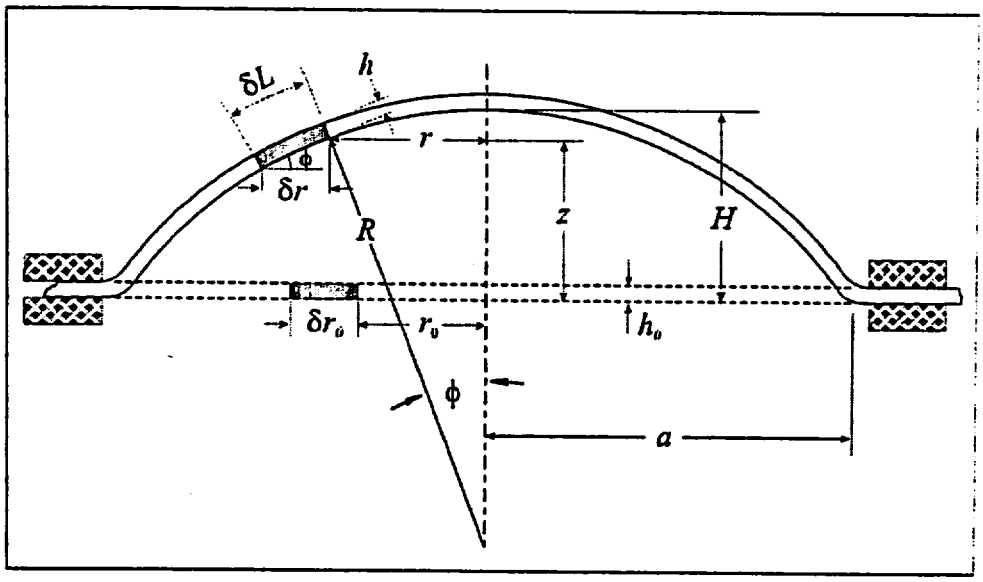

Fig. 13. Spherical geometry of deformation assumed in plastic instability theory [8].

The quantile curves shown in Fig. 12b are determined from the LogLaplace stochastic model developed in [1] and scaled by the burst pressure predictions from the Chakrabarty and Alexander model [8] using a diaphragm thickness of 0.24 in. and the bounding stress-strain curve shown in Fig. 4. With the service pressure, SP, as the random variate, the three-parameter Log-Laplace continuous distribution has the following probability density function, f_{LP}, and cumulative distribution function, F_{LP},

$$f_{LP}(SP\,|\,a,b,c)=\begin{cases}\dfrac{c}{2b}\left(\dfrac{SP-a}{b}\right)^{c-1} & ;\ a<SP<b\\ \dfrac{c}{2b}\left(\dfrac{SP-a}{b}\right)^{-c-1} & ;\ SP\geq b\end{cases}\qquad \text{for } a\geq 0,\ (b,c)>0$$

$$\Pr(X\leq SP)=F_{LP}(SP\,|\,a,b,c)=\begin{cases}\dfrac{1}{2}\left(\dfrac{SP-a}{b}\right)^{c} & ;\ a<SP<b\\ 1-\dfrac{1}{2}\left(\dfrac{SP-a}{b}\right)^{-c} & ;\ SP\geq b\end{cases}\qquad \text{for } a\geq 0,\ (b,c)>0 \tag{2}$$

and the percentile function (inverse cumulative distribution function) is

$$Q_{LP}(p\,|\,b,c)=$$

$$BP_p=\begin{cases}a+\exp\left[\ln(b)+\dfrac{\ln(2p)}{c}\right] & ;p\leq 0.5\\ a+\exp\left[\ln(b)-\dfrac{\ln\left[2(1-p)\right]}{c}\right] & ;p>0.5\end{cases}\qquad \text{for } (0<p<1) \tag{3}$$

where BP_p is the predicted burst (failure) pressure with probability p, a is the location parameter, b is the scale parameter, and c is the shape parameter. The fitted parameters from [1] were:

$$\begin{aligned} a &= 0 \\ b &= 1.1057 \times P_{model} \\ c &= 11.45441 \end{aligned} \tag{4}$$

where P_{model} can either be the *pressure at numerical instability*, P_{NI}, calculated from a finite-element model based on a given cavity configuration and cladding thickness or the burst pressure calculated from the center membrane theoretical model of Chakrabarty and Alexander [8] (see Fig. 12b). The median predicted failure pressures given in Table 3 are calculated from the P_{NI} values by observing from Eq. (3) that

$$\text{median predicted failure pressure} = BP_{0.5} = b \times P_{NI} = 1.1057 \times P_{NI} \tag{5}$$

For the bounded "as-found" case, the median failure pressure is 7.35 ksi for a cladding thickness of 0.24 in. and 5.73 ksi for a cladding thickness of 0.1825 in.

The diaphragm areas in Table 4 correspond to two service pressures, an operating pressure of 2.165 ksi and a safety-valve set-point pressure of 2.5 ksi. The cumulative failure probabilities are scaled from the predictions of the Chakrabarty and Alexander [8] theoretical model with a diaphragm thickness of 0.24 in. and the bounding SS 308 stress-strain curve from Fig. 4.

Table 4. Diaphragm Areas at Two Pressures Over a Range of Failure Probabilities

Cumulative Failure Probability	Required Diaphragm Area	
	Operating Pressure[1] (in^2)	Set-Point Pressure[2] (in^2)
1%	164.4	123.3
5%	217.7	163.3
50%	325.4	244.0
95%	486.4	364.8
99%	644.3	483.2

[1] Operating pressure = 2.165 ksi

[2] Safety-valve set-point pressure = 2.5 ksi

Diaphragm thickness = 0.24 in.

SS 308 Cladding properties

5 Summary and Conclusions

This report has presented the results of finite-element analyses (using the submodeling techniques available in the ABAQUS computer code) of the Davis-Besse RPV head in the region of the wastage area around Nozzle 3. These finite-element analyses applied a nonlinear finite-strain procedure with an incrementally increasing pressure load applied from zero up to the load at which numerical instabilities caused ABAQUS to abort the execution. The internal pressure attained immediately preceding the onset of numerical instability is designated as the *pressure at numerical instability*, P_{NI} [1]. For a bounding calculation of the "as-found" condition, the P_{NI}, was calculated to be 6.65 ksi. Depending on the shape of the wastage footprint, the required exposed-cladding area for the P_{NI} to occur at an operating pressure of 2.165 ksi ranged from approximately 254 in.^{2} to 280 in.^{2}. The application of a vertical constraint to the top of Nozzle 11 (see the Ellipsoidal Case 20a* in Table 3) produced a small increase in the value of P_{NI}. The center-membrane theory of burst pressure for circular diaphragms produced trends (as a function of effective diaphragm area under load) that followed the observed trends for the irregular geometries of the growth-pattern wastage areas investigated in the current study. Associated cumulative probabilities are provided based on a stochastic model described in a previous report [1]. For the bounded "as-found" case, the median predicted failure pressure, $BP_{0.5}$, is 7.35 ksi for a cladding thickness of 0.24 in. and 5.73 ksi for a cladding thickness of 0.1825 in. For $BP_{0.5}$ equal to 2.165 ksi, the center-membrane theory estimates a required diaphragm area of 325.4 in^2 with a cladding thickness of 0.24 in. The value of 0.24 in. is the minimum cladding thickness obtained from UT measurements of the wastage area based on a ½ inch grid as depicted in Fig. 14 of ref. [4].

Estimates of failure pressure with associated probabilities can be calculated for a broad range of exposed cladding areas from the theoretical treatment of circular diaphragms due to Chakrabarty and Alexander [8] in conjunction with the stochastic model described in a previous report [1]. The thin-walled membrane assumptions applied in the theory appear to better approximate the conditions in the exposed cladding as the wastage area increases in size. As can be observed in Fig. 12, the shape of the footprint approaches a second-order effect as the footprint area increases.

At the time of this writing, data from a "dental" molding of the wastage-area cavity became available. Figure 14 compares the footprint derived from a photograph of this molding with the footprint used in these analyses obtained from [4]. It can be observed from Fig. 14 that the wastage area assumed in this report is conservatively larger than the footprint estimated from the recent molding.

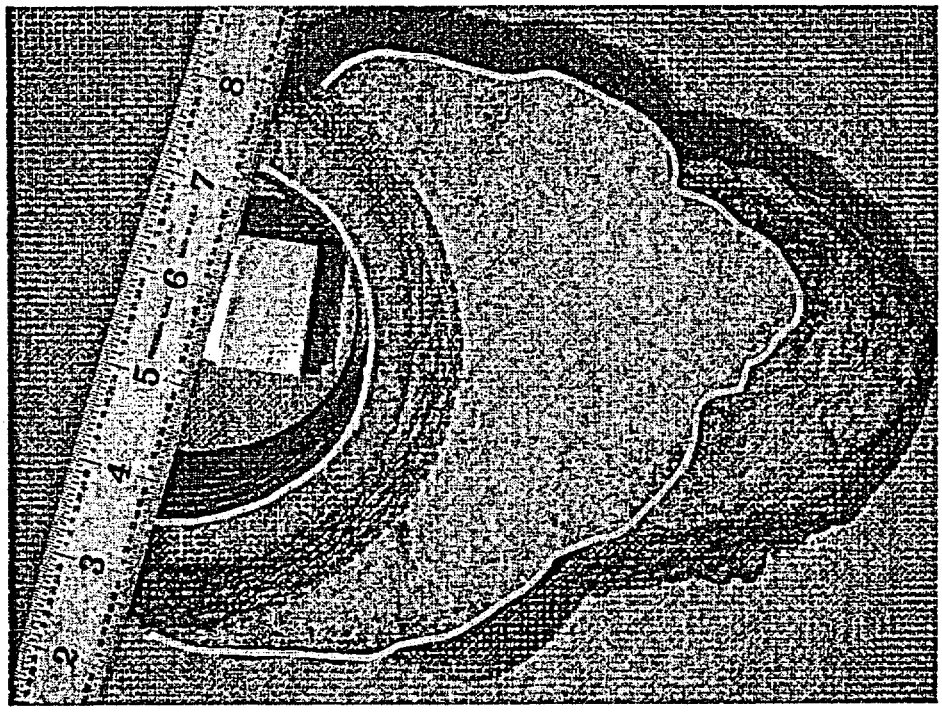

Magnification: 6"/3.82" = 1.57X

(a) Area of photo: (6")(1.57) x (4.5")(1.57X) = 66.55 in^2

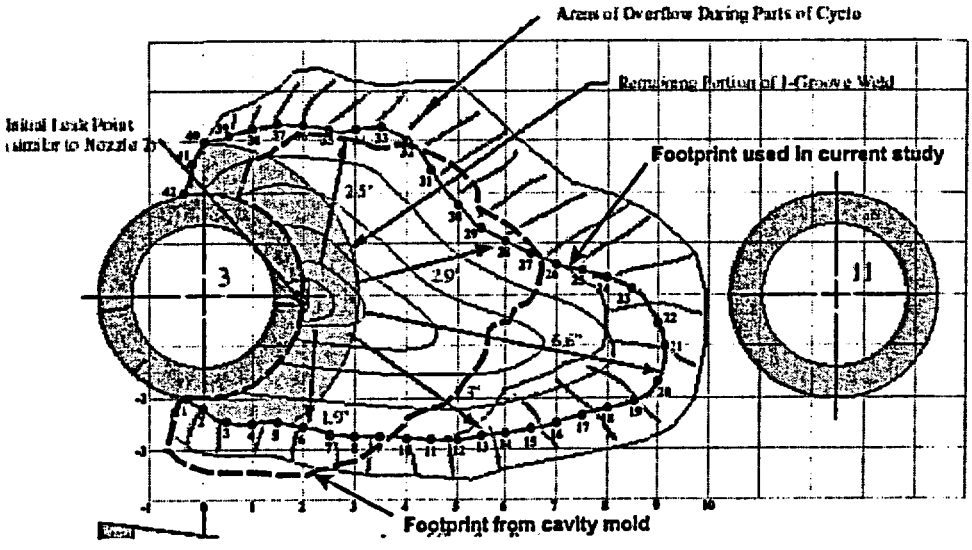

(b)

Fig. 14. Comparison of recent characterization of wastage-area footprint with geometry used in the current study: (a) photograph of cavity mold and (b) footprint used in current study and footprint estimated from cavity mold.

References

1. P. T. Williams and B. R. Bass, *Stochastic Failure Model for the Davis-Besse RPV Head*, ORNL/NRC/LTR-???, under review.
2. NRC Bulletin 2001-01, "Circumferential Cracking of Reactor Pressure Vessel Head Penetration Nozzles", August 3, 2001.
3. *Recent Experience with Degradation of Reactor Pressure Vessel Head*, NRC Information Notice 2002-11, United States Nuclear Regulatory Commission, Office of Nuclear Reactor Regulation, Washington, DC, March 12, 2002.
4. S. A. Loehlein, *Root Cause Analysis Report, Significant Degradation of Reactor Pressure Vessel Head*, CR 2002-0891, Davis-Besse Power Station, April 15, 2002.
5. Personal communication with Computational Mechanics Corporation of Columbus, Columbus, OH, March 2002, Data from PIFRAC database.
6. *Nuclear Systems Materials Handbook*, Vol. 1, Design Data, Section 1A for 308/308L weld, Table II.
7. *ABAQUS/Standard User's Guide, Volume I*, v6.2-4, Hibbitt, Karlsson, and Sorensen, Inc., Pawtucket, RI, 2001.
8. J. Chakrabarty and J. M. Alexander, "Hydrostatic Bulging of Circular Diaphragms," *J. Strain Anal.* 5(3), (1970) 155-161.
9. R. Hill, "A Theory of the Plastic Bulging of a Metal Diaphragm by Lateral Pressure," *Philos. Mag. (Ser. 7)* 41, (1950) 1133.